UNIVERSITE BLAISE PASCAL IN2P3/CNRS

LABORATOIRE DE PHYSIQUE CORPUSCULAIRE

63177 AUBIERE CEDEX TELEPHONE : 73 40 72 80

TELECOPIE : 73 26 45 98

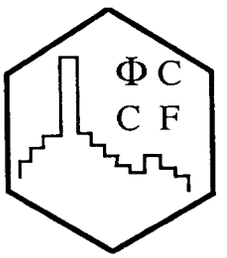

STUDY OF IN-MEDIUM EFFECTS WITH THE AU + AU FOPI DATA AT 400 A.MEV

V. RAMILLIEN, P. DUPIEUX, J.P. ALARD, V. AMOUROUX, N. BASTID, L. BERGER, S. BOUSSANGE, L. FRAYSSE, M. IBNOUZAHIR, G. MONTAROU, I. MONTBEL, P. PRAS

Laboratoire de Physique Corpusculaire de Clermont-Ferrand
IN2P3/CNRS - Université Blaise Pascal
F-63177 AUBIERE CEDEX FRANCE

and

FOPI - COLLABORATION

PCCF RI 9413

STUDY OF IN-MEDIUM EFFECTS WITH THE AU + AU FOPI DATA AT 400 A.MEV

V.Ramillien[1], P.Dupieux[1], J.P.Alard[1], V.Amouroux[1], N.Bastid[1], L.Berger[1], S.Boussange[1], L.Fraysse[1], M.Ibnouzahir[1], G.Montarou[1], I.Montbel[1], P.Pras[1], Z.Basrak[13], I.M.Belayev[8], M.Bini[5], Th.Blaich[7], A.Buta[2], R.Caplar[13], C.Cerruti[11], N.Cindro[13], J.P.Coffin[11], R.Donà[11], J.Erö[3], Z.G.Fan[4], P.Fintz[11], Z.Fodor[3], R.Freifelder[4], S.Frolov[8], A.Gobbi[4], Y.Gregorian[9], G.Guillaume[11], C.Hartnack[14], N.Herrmann[6], K.D.Hildenbrand[4], S.Hölbling[13], A.Houari[11], S.C.Jeong[4], F.Jundt[11], J.Kecskemeti[3], P.Koncz[3], Y.Korchagin[8], R.Kotte[10], M.Krämer[4], C.Khun[11], I.Legrand[2], A.Lebedev[8], C.Maguire[11], V.Manko[9], P.Maurenzig[5], G.Mgebrishvili[9], J.Mösner[10], D.Moisa[2], W.Neubert[10], A.Olmi[5], G.Pasquali[5], D.Pelte[6], M.Petrovici[2], G.Poggi[5], F.Rami[11], W.Reisdorf[4], A.Sadchikov[9], D.Schüll[4], Z.Seres[3], B.Sikora[12], V.Simion[2], S.Smolyankin[8], U.Sodan[4], K.Teh[4], R.Tezkratt[11], M.Trzaska[6], M.A.Vasiliev[9], P.Wagner[11], J.P.Wessels[4], T.Wienold[4], Z.Wilhelmi[12], D.Wohlfarth[10], A.V.Zhilin[8]

FOPI-Collaboration

[1] Laboratoire de Physique Corpusculaire, IN2P3-CNRS, Université Blaise Pascal, Clermont-Fd, France

[2] Institute for Physics and Nuclear Engineering, Bucharest, Romania

[3] Central Research Institute for Physics, Budapest, Hungary

[4] Gesellschaft für Schwerionenforschung, Darmstadt, Germany

[5] Università and Istituto Nazionale di Fisica Nucleare, Florence, Italy

[6] Physikalisches Institut der Universität Heidelberg, Heidelberg, Germany

[7] Universität Mainz, Mainz, Germany

[8] Institute for Experimental and Theoretical Physics, Moscow, Russia

[9] Kurchatov Institute for Atomic Energy, Moscow, Russia

[10] Forschungszentrum, Rossendorf, Germany

[11] Centre de Recherche Nucléaire, IN2P3-CNRS, Université Louis Pasteur, Stras-

bourg, France

(12) Institute of Experimental Physics, Warsaw University, Warsaw, Poland

(13) Rudjer Boskovic Institute, Zagreb, Croatia

(14) SUBATECH Nantes, France

abstract : *We present new experimental data obtained with the FOPI detector at SIS, for the Au + Au heavy ion collisions at 400 A.MeV incident energy. The sideward flow, determined from a method without reaction plane reconstruction, and the nuclear stopping are studied as a function of the centrality of the collisions. In order to study the nuclear in-medium effects, which act on the N-N cross-sections and potential and hence on experimental observables like the nuclear matter flow and stopping, these results are compared with the predictions of two different QMD versions. The first one offers a fully microscopic calculation of the cross-sections and potential in the G-matrix formalism and naturally includes the in-medium effects (this version is for the first time confronted to experiment). The second one uses a standard Skyrme potential plus a momentum dependent term in order to mimic the in-medium effects.*

key words : Heavy ion reactions, Equation of state, Transverse momentum transfert, In-medium effects, Quantum Molecular Dynamic model, G-matrix

1. INTRODUCTION

One of the principal goals of the study of heavy ion reactions at intermediate energies of a few hundreds of MeV per nucleon is the determination of the nuclear matter equation of state (EOS). The EOS is defined as the dependence of the nucleon binding energy on the density ρ and the temperature T of the nuclear medium, although the temperature dependence is often neglected. The EOS can be roughly characterized by the compressibility coefficient K. We usually assume K $\approx$ 200 MeV for a Soft EOS and K $\approx$ 380 MeV for a Hard EOS. The strategy in extracting the nuclear EOS is to compare experiments and models for variables sensitive to compressionnal effects. The most studied one is the transverse momentum transfert in the reaction plane for central or semi-central collisions, the so-called sideward flow (for experimental results see [1-5]). The sensitivity of such an observable is however limited and the conclusions concerning the EOS can be easily modified. In particular, the nuclear in-medium effects like the density and momentum dependence of the nucleon-nucleon (N-N) cross-sections and potential[6-8] have to be properly treated.

In this paper, we try to evaluate how accurately some modern transport theories reproduce these in-medium effects on the sideward flow and nuclear matter stopping power (these observables being obviously strongly correlated). To achieve this goal, we compare the Au + Au data at 400 MeV per nucleon incident energy of the FOPI detector with the G-matrix Quantum Molecular Dynamic model GQMD [7,9] which includes these in-medium effects. The same data are also compared with the "Isospin" QMD (IQMD) [10] results where the free N-N cross-sections (Cugnon parametrization) are used together with a Soft Skyrme potential supplemented with a momentum dependent interaction (MDI) proportional to ρ (this version is noted IQMDSM). Such a phenomenological potential is introduced to reproduce the in-medium effects and it can be questionable whether such a parametrization is sufficient or not.

2. EXPERIMENTAL SETUP

The data were obtained with the phase-I setup of the FOPI detector [11] which covers the polar angles between 1.2-30 degrees in the full azimuthal plane. A wall of 512 plastic scintillator strips and a gas cluster detector cover the external part of FOPI between 7-30 degrees. The inner part, between 1.2-7 degrees, is composed of 252 scintillator paddles of

trapezoïdal shape, also supplemented with an additional cluster detector. The two walls give a time of flight and energy loss information for each particle of sufficient energy. The cluster detectors identify the heavy fragments of slow velocity stopped in the scintillators of the walls. We finally obtain the charge and the velocity of each particle.

The analysis has been limited to the fragments of charge $Z \leq 10$ detected in these two sets. The detection thresholds amount to roughly 14 A.MeV for Z=1 and 35 A.MeV for Z=10 fragments in the external part of the detector and are slightly higher in the inner part.

3. THE G-MATRIX QMD MODEL

The GQMD model [9] includes the in-medium effects starting from a bare N-N interaction (Reid potentials [12]). The N-N cross-sections and potential are then deduced in the G-matrix formalism microscopically in a consistent way (they are not independent). The resulting EOS has a compressibility K=182 MeV and the saturation point is found at $\rho = 0.2$ fm^{-3} with a binding energy of -16 MeV. There is no free parameter and the difference with the known ground state value of infinite nuclear matter (binding energy = -16 MeV at normal density $\rho_0 = 0.17$ fm^{-3}) can be explained by the non-relativistic G-matrix treatment [8].

At 400 MeV per nucleon incident energy, we do not expect a large difference between the free and the G-matrix cross-sections because the influence of the Pauli blocking is small [8]. This is also confirmed in ref. [7] where only differences on the number of collisions per nucleon are found to be relevant between these two kinds of cross-sections. On the other hand, the G-matrix potential U(ρ,p) has been compared in ref. [7] to a Skyrme parametrization with almost the same compressibility and a momentum dependent term. U(ρ,p) is stronger at low density (higher momentum dependence of the G-matrix) but the Skyrme potential has a stronger density dependence even with the same compressibility coefficient. This comparison shows an appreciably more important sideward flow in GQMD for the system Nb + Nb at 400 MeV per nucleon. The differences in the initializations (see details in ref. [8,9]) between these two QMD versions are responsible for a part of this discrepancy. However for the considered Au + Au system this discrepancy is not as large as the one in the Nb + Nb reaction [13]. This problem does not occur between GQMD and IQMD where the initializations are similar.

This microscopic model has never been confronted with experimental data because nuclei in the calculation are not stable anymore after 60 fm/c. At this time, only dynamical observables like the nuclear flow or stopping have reached their asymptotic values but the fragment formation is not reliable and that creates difficulties to compare with exper-

iment. We have overcome these difficulties in always comparing quantities weighted by the fragment charge Z (so called proton-like analysis) for the experimental data and the IQMD model . The centrality criterion has also been calculated from dynamical quantities (we cannot use for instance a multiplicity criterion). We have performed many checks probing the validity of the comparison in such conditions. We will discuss these tests in more details in the following (filter problems in particular).

4. EXPERIMENTAL METHOD AND RESULTS

Among the Au + Au FOPI data from 100 to 1050 A.MeV incident energy, we have chosen to study the 400 A.MeV one. This energy is considered to be the highest one which can be compared with a non-relativistic model like GQMD that does not include the production of pions. We however still expect a dependence of the observables on the EOS (densities of 2-3 ρ_0 are reached in central collisions) and the contribution of fragments is already small at such energy (a few percent on the flow for instance).

We present only the central trigger events which require a high multiplicity in the external wall of the detector and are not affected by the background. This trigger roughly selects impact parameters lower than 9 fm. The calculations are passed through the geometrical (including energy thresholds) FOPI filter before being compared with experiment.

The N-N cross-sections and potential influence both the flow and the nuclear stopping so we have to compare this two quantities between experiment and models. For the nuclear matter stopping, we have chosen to show the rapidity distributions and the cross-section of the variable called $ERAT$.

$ERAT$ is defined as the ratio of the transversal to the longitudinal kinetic energy for the i particles of an event with rapidity y_i greater than center of mass rapidity y_{cm} (y_{cm} = 0.44 for 400 A.MeV incident energy):

$$ERAT = \left(\sum_i E_i^{\perp} / \sum_i E_i^{//} \right)_{y_i > y_{cm}} \qquad (1)$$

Although $ERAT$ offers the advantages of a global variable to characterize the stopping, it is strongly distorted by the experimental filter and the 30° cut of the detector in particular.

We show in figure I the differential cross-section $d\sigma/d(ERAT)$. For $ERAT > 0.3$, we find a good qualitative agreement between experiment and both IQMDSM and GQMD (normalized to the geometrical cross-section $\sigma_g = \pi\, b_{max}^2 = 6157$ mb with $b_{max} = 14$ fm) although the calculations systematically overestimate the experimental results. This discrepancy can not be explained by filter effects alone and we will see more details in the

rapidity distributions. For $ERAT < 0.3$, the experimental distribution is strongly affected by the trigger effects. Moreover in a simulation like GQMD, where the projectile remnant is not formed, very low $ERAT$ values can not be reached. The detector cut at small polar angles, which removes the projectile remnant, does not play as well on individual nucleons which can have some transversal momentum and artificially fit the acceptance and hence increase the $ERAT$ value (see the difference between the two models on figure I for low $ERAT$). For these two reasons, we have in the following limited the comparison to $ERAT > 0.3$.

We also use $ERAT$ to select different centrality classes of events. This is strongly supported by QMD simulations which indicate a strong correlation between $ERAT$ and the impact parameter b although the $ERAT$ values are strongly sensitive to the experimental filter. We have divided both the experimental and simulated $ERAT$ distributions in 4 classes (see table I for the impact parameter correspondence in the models). The integrated cross-sections σ_{int} for $ERAT > 0.3$ are the following :

$\sigma_{int}^{Exp} = 1090$ mb ; $\sigma_{int}^{GQMD} = 1440$ mb and $\sigma_{int}^{IQMDSM} = 1515$ mb.

We show, in figure II, the rapidity distributions dN/dy_0 for proton-like particles in the different $ERAT$ classes previously defined. y_0 is the reduced rapidity defined as :

$$y_0 = (y - y_{cm})/y_{cm} \tag{2}$$

$y_0 = 0$ for particles of laboratory rapidity $y = y_{cm}$ and $y_0 = 1$ for projectile rapidity.

We clearly observe a shift towards mid-rapidity when going to more central collisions and the models generally reproduce the experimental trends (some filter problems for GQMD in the more peripheral $ERAT$ class can still be seen). Larger y_0 values are systematically reached in the data as compared to the models. This obviously corresponds to the discrepancy observed on the $ERAT$ cross-section but the origin of these particles with large rapidity is not yet clear (we can think to some special combinations of the Fermi momenta during the collision process).

We study sideward flow from the method without reaction plane reconstruction [14]. The main advantages of this method are that it does not need a correction of finite number effects and it permits an estimate and a correction of the energy and momentum conservation effects. This method is based on the momentum correlations due to the collective motion in the reaction plane. The correlations are supposed to come only from the flow and conservation effects. In this case, for two particles μ and ν of the same event, with transverse momenta $\vec{p}_\mu^{\,t}$ and $\vec{p}_\nu^{\,t}$ per unit of mass and reduced rapidities y_{0_μ} and y_{0_ν}, we

can write :

$$< \vec{p}_\mu^{\,t}(y_{0_\mu})\ \vec{p}_\nu^{\,t}(y_{0_\nu}) > = < p_\mu^x(y_{0_\mu}) > < p_\nu^x(y_{0_\nu}) > \ - \alpha \ < p_\mu^{t^2}(y_{0_\mu}) > < p_\nu^{t^2}(y_{0_\nu}) > \quad (3)$$

In this formula, p^x is the projection in the true reaction plane of $\vec{p}^{\,t}$ and $< p^x >$ represents the sideward flow. α is an additional recoil term which takes into account the conservation effects :

$$\alpha \approx [< \sum p^{t^2} >_{event}]^{-1} \quad (4)$$

(the complete expression of α can be found in ref. [2]). The formula (3) can be developed in order to derive an exploitable expression of the flow :

$$< p^x(y_0) >= \frac{< Z_\mu \vec{p}_\mu^{\,t}(y_{0_\mu}) \omega_\nu Z_\nu \vec{p}_\nu^{\,t} >_{\mu \neq \nu} + \alpha < Z_\mu p_\mu^{t^2}(y_{0_\mu}) >< Z_\nu \omega_\nu p_\nu^{t^2} >}{\sqrt{< Z_\nu \omega_\nu \vec{p}_\nu^{\,t} Z_\mu \omega_\mu \vec{p}_\mu^{\,t} >_{\mu \neq \nu} + \alpha < Z_\nu \omega_\nu p_\nu^{t^2} >^2}} \quad (5)$$

The momenta are weighted by the fragment charge in the framework of this proton-like analysis. ω is only introduced to reduce the fluctuations around y_{cm} :

$$\omega = \begin{cases} +1 & \text{for } y_{0_\nu} > 0.3 \\ 0 & \text{for } |y_{0_\nu}| \leq 0.3 \\ -1 & \text{for } y_{0_\nu} < -0.3 \end{cases} \quad (6)$$

The error bars represented on the following figures (if they are greater than the symbol size) are purely statistical.

We give in figure III, left panel, the experimental distributions $< p^x(y_0) >$ for $\alpha = 0$ and α calculated with (4) for central collisions without additional $ERAT$ selection. We will discuss in more details the apparatus effects on these curves, but we can already mention that only the positive rapidity part has to be regarded. In the positive mid-rapidity part, the flow has almost the typical linear dependence on rapidity followed by a bump around the projectile rapidity. Comparing the curve $\alpha = 0$ to $\alpha \neq 0$, we can see that the energy and momentum conservation effects are very small. This can be easily explained by the high multiplicity obtained in Au on Au collisions and also by the strength of the collective flow. Moreover α should be calculated with the particles of the whole event instead of only those within the FOPI acceptance: in this sense, α is overestimated here and the conservation effects on the flow should be even lower. Consequently, we neglect in the following these effects and we calculate the flow for $\alpha = 0$.

In figure III, right panel, we compare the flow in different centrality bins. We observe that the slope around mid-rapidity (the so-called flow parameter F) is rather insensitive to

the centrality selection. A more detailed analysis with FOPI [4] shows that, in this range of impact parameter, F has reached its maximum (F should decrease for smaller and larger impact parameters) and that the values are in good agreement with those of the Plastic Ball [1,4].

The shape of the curves around the projectile rapidity is more affected by these centrality selections. The observed bump in the most peripheral $ERAT$ class tends to disappear when going to more central ones.

Before confronting the experimental data to the GQMD predictions, we have verified with a QMD model that dynamical observables and the flow in particular do not evolve anymore between 60 and 200 fm/c. We have also compared the flow before and after fragment formation in this QMD simulation. For $ERAT > 0.3$, only a very small influence on these tests has been observed. For $ERAT < 0.3$, the fact that the projectile remnant is not formed tends to lower the flow in the projectile rapidity region (see also the effect on $ERAT$ previously described). We have also studied in details the acceptance effects on the flow by filtering simulated events through the geometrical and the complete FOPI filter. This later uses the GEANT-CERN software facility and includes the modular description of the detector which allows in particular the simulation of double-hits. The results given by these two filters are very closed. The complete filter however explains the little rapidity shift at $< p^x > = 0$ one can observe on the experimental distributions (fig.III). The geometrical filter effects are shown in figure IV on the GQMD flow patterns. The cuts affect only slightly the distributions $< p^x(y_0) >$ for the positive rapidities.

All these tests give us confidence in the comparison of the experimental $< p^x(y_0) >$ with GQMD and IQMDSM predictions, filtered through the geometrical filter, presented in figure V for the different centrality classes. There is a generally good agreement between the two models for all $ERAT$ bins. They also fit the data in the mid-rapidity region (except maybe GQMD in the first $ERAT$ bin which slightly deviates from the data). In all cases, the flow is a little bit underestimated around the projectile rapidity. The same analysis was done with IQMD, a Hard EOS plus MDI (IQMDHM). The same trends were observed, except that a better agreement was found in central event classes around the projectile rapidity. The sensitivity to the EOS was found to be rather small.

As suggested in ref. [3], we have finally studied $< p^x(ERAT) >$, integrating on the y_0 distribution (positive part only) for various $ERAT$ bins. $< p^x(ERAT) >$ represents the total amount of sideward flow in the forward center of mass hemisphere as a function of the centrality. It has the advantage to be a global variable and the main differences between experiment and models stand out more clearly in such a representation. The full detector bias on $< p^x(ERAT) >$ is estimated to be less than 10% (see also ref. [3]).

We present on figure VI the comparison between experimental $< p^x(ERAT) >$,

GQMD, IQMDSM and IQMDHM. The experimental curve presents a maximum around $ERAT = 0.5$ (b$\approx$4 fm). As can be deduced from the previous picture, all the model predictions underestimate the total amount of flow, except as mentioned earlier, IQMDHM for large $ERAT$ values. Closely comparing the predictions of the models, among themselves and relatively to the experiment, we can extract some clear conclusions :

• for $ERAT < 0.4$, the density effects are still low and the momentum dependence of the interaction dominates. As it is well known, the one in GQMD is stronger and fits better the data (moreover the first point for GQMD at $ERAT = 0.25$ is already distorted, due to the fact that the projectile remnant cannot be formed, and we would expect to find this point even closer to the data).

• for $ERAT$ values > 0.7, the density effects are also important and in this case the Hard EOS leads to more directed flow and reproduces the data. The microscopic model clearly lacks density dependence (as a consequence, this also shifts the maximum to a lower $ERAT$ value).

• comparing GQMD and IQMDSM, we can see that the momentum dependence of GQMD is higher than the one of IQMDSM (see point 1). For large $ERAT$, the two models give however the same flow. Combining these two informations, this confirms the fact that the density dependence of GQMD is lower although its compressibility coefficient is closed to the one of IQMDSM.

All these comparisons between the models are fully supported by the direct study of $< p^x(b) >$ (b impact parameter). What is more the study of $< p_x(b) >$ indicates that the difference between GQMD and IQMDSM really shows up for b > 6 fm due to the different treatments of the MDI. Unfortunately this impact parameter corresponds more or less to the point where our comparison with experimental data must be stopped (see comments for the first point at $ERAT = 0.25$ for GQMD).

5. CONCLUSION

We have presented new experimental results concerning the stopping and the sideward flow in Au + Au at 400 A.MeV collisions.

We find that the experimental stopping is overestimated from 30−40 % by IQMDSM and GQMD.

Concerning the sideward flow, a generally good agreement is at first observed between GQMD and IQMDSM, better than the one expected from ref. [7], due to the now matched initializations. However, the momentum dependence of GQMD is somewhat stronger as can be seen for the more peripheral collisions and fits better the data. Unfortunately

the fact that the projectile remnant cannot be formed in GQMD forbids us to push the comparison to really peripheral events where the sensitivity is better. On the other hand, the microscopic model clearly lacks density dependence to reproduce the more central events but this is a well known characteristic of this QMD version. The phenomenological potential associated to the free N-N cross-sections also gives a good representation of the experimental flow and stopping. Looking in more details, the Hard Skyrme potential is needed to reproduce the flow in the more central events but either the Hard or the Soft version fails in case of the more peripheral ones. This is due to a too weak momentum dependence but a recent parametrization of the optical potential, proposed in ref. [15], concludes to a higher repulsion with the new values.

Finally we want to stress that the sensitivity to the EOS is small and a really accurate treatment of the in-medium effects in particular, both for the potential and the cross-sections, would be necessary to conclude in favour of a given EOS.

We would like to thank Prof. J.Aichelin for enlightening discussions.

We also would like to thank Prof. A.Faessler and his group for cross-checks of simulation results and for their fruitfull comments on this work.

references :

(1) H.A.Gustafsson, H.H.Gutbrod, J.Harris, B.V.Jacak, K.H.Kampert, B.Kolb, A.M.Poskanzer, H.G.Ritter, H.R.Schmidt, Mod. Phys. Lett. A3 (1988) 1323

(2) M.Demoulins, Thesis at Univ. Paris Sud (1989)

(3) T.Wienold, thesis, GSI Rep. 93 28 (1993)
T.Wienold et al., to be published in Phys. Rev. Lett.

(4) F.Rami, R.Donà, C.Cerruti, J.P.Coffin, P.Fintz, G.Guillaume, A.Houari, F.Jundt, C.Kuhn, P.Wagner, for the FOPI collaboration GSI Rep. (1993) 19

(5) Q.Pan, P.Danielewicz, Phys. Rev. Lett. 70 (1993) 2062

(6) M.Trefz, A.Faessler, W.H.Dickhoff, Nucl. Phys. A443 (1985) 499

(7) Dao T.Khoa, N.Ohtsuka, M.A.Matin, A.Faessler, S.W.Huang, E.Lehmann, R.K.Puri, Nucl. Phys. A548 (1992) 102

(8) J.Aichelin, Phys. Rep. 202 (1991) 233 and ref. therein

(9) J.Jaenicke, J.Aichelin, N.Ohtsuka, R.Linden, A.Faessler, Nucl. Phys. A536 (1992) 201

(10) C.Hartnack, thesis, GSI Rep. 93 05 (1993),
C.Hartnack, Phys. Lett. B336 (1994) 131

(11) A.Gobbi, J.P.Alard, G.Augustinski, Z.Basrak, N.Bastid, I.M.Belayev, T.Blaich, P.Boccaccio, R.Bock, S.Boussange, A.Buta, R.Caplar, C.Cerruti, R.J.Charity, N.Cindro, J.P.Coffin, M.Crouau, F.Daudon, J.F.Devin, P.Dupieux, J.Erö, Z.G.Fan, C.Fayard, P.Fintz, Z.Fodor, L.Fraysse, R.Freifelder, S.Frolov, E.Gimenez, Y.Grigorian, G.Guillaume, N.Herrmann, K.D.Hildenbrand, S.Hölbling, F.Hornecker, A.Houari, S.C.Jeong, M.Jorio, F.Jundt, J.Kecskeméti, P.Konck, Y.Korchagin, R.Kotte, M.Krämer, C.Kuhn, A.Lebedev, I.Legrand, C.F.Maguire, V.Manko, M.Marquardt, T.Matulewicz, S.Mayade, G.Mgebrishvili, J.Mösner, D.Moisa, G.Montarou, I.Montbel, P.Morel, W.Neubert, R.Neunlist, G.Ortlepp, D.Pelte, M.Petrovici, F.Rami, W.Reisdorf, M.A.Saettel, E.Sahuc, G.Savinel, Z.Seres, D.Schüll, B.Sikora, V.Simion, S.Smolyankin, U.Sodan, M.H.Tanaka, K.M.Teh, R.Tezkratt, B.Tischler, M.Trzaska, M.A.Vasiliev, D.Vincent, P.Wagner, J.Weinert, J.P.Wessels, T.Wienold, Z.Wilhelmi, D.Wohlfarth, A.V.Zhilin, N.I.M. A324 (1993) 156

(12) R.V.Reid Jr, Ann. of Phys. 50 (1968) 411

(13) E.Lehmann, private communication (1994)

(14) P.Danielewicz, H.Ströbele, G.Odyniec, D.Bangert, R.Bock, R.Brockmann, J.W.Harris, H.G.Pugh, R.E.Renfordt, A.Sandoval, D.Schall, L.S.Schroeder, R.Stock, Phys. Rev. C38 (1988) 120

(15) C.Hartnack, Internal Report LPN 93 13, Univ. Nantes

figure captions :

figure I : differential cross-sections $d\sigma/d(ERAT)$. Comparison between experimental FOPI data and the models GQMD and IQMDSM for the system Au + Au at 400 MeV per nucleon.

figure II : rapidity distributions dN/dy_0 for different centrality selections (see table I). Comparison between experiment, GQMD and IQMDSM for the system Au + Au at 400 MeV per nucleon.

figure III : experimental distributions of $< p^x(y_0) >$ for proton-like particles and for the system Au + Au at 400 MeV per nucleon.
The left panel presents the results with ($\alpha \neq 0$) and without ($\alpha = 0$) correction of the energy and momentum conservation effects (see text).
The right panel shows the variation of $< p^x(y_0) >$ with the centrality of the events.

figure IV : $< p^x(y_0) >$ distributions obtained with the GQMD calculation with and without the geometrical FOPI filter effects, for the system Au + Au at 400 MeV per nucleon.

figure V : $< p^x(y_0) >$ distributions for the system Au + Au at 400 MeV per nucleon. Comparison between experimental FOPI distributions and the models GQMD and IQMDSM.

figure VI : $< p^x(ERAT) >$ distributions for the system Au + Au at 400 MeV per nucleon. Comparison between experimental FOPI distributions and the models GQMD, IQMDSM and IQMDHM.

table caption :

Table I : Mean values and standard deviations of the impact parameter in GQMD and IQMDSM for various $ERAT$ classes.

$ERAT$	b^{GQMD}	b^{IQMDSM}
$.30 \leq ERAT < .43$	6.0 ± 1.3	6.2 ± 1.4
$.43 \leq ERAT < .58$	3.9 ± 1.3	4.5 ± 1.1
$.58 \leq ERAT < .72$	2.4 ± 1.2	3.1 ± 1.2
$ERAT \geq .72$	1.3 ± 0.9	1.5 ± 1.0

table I

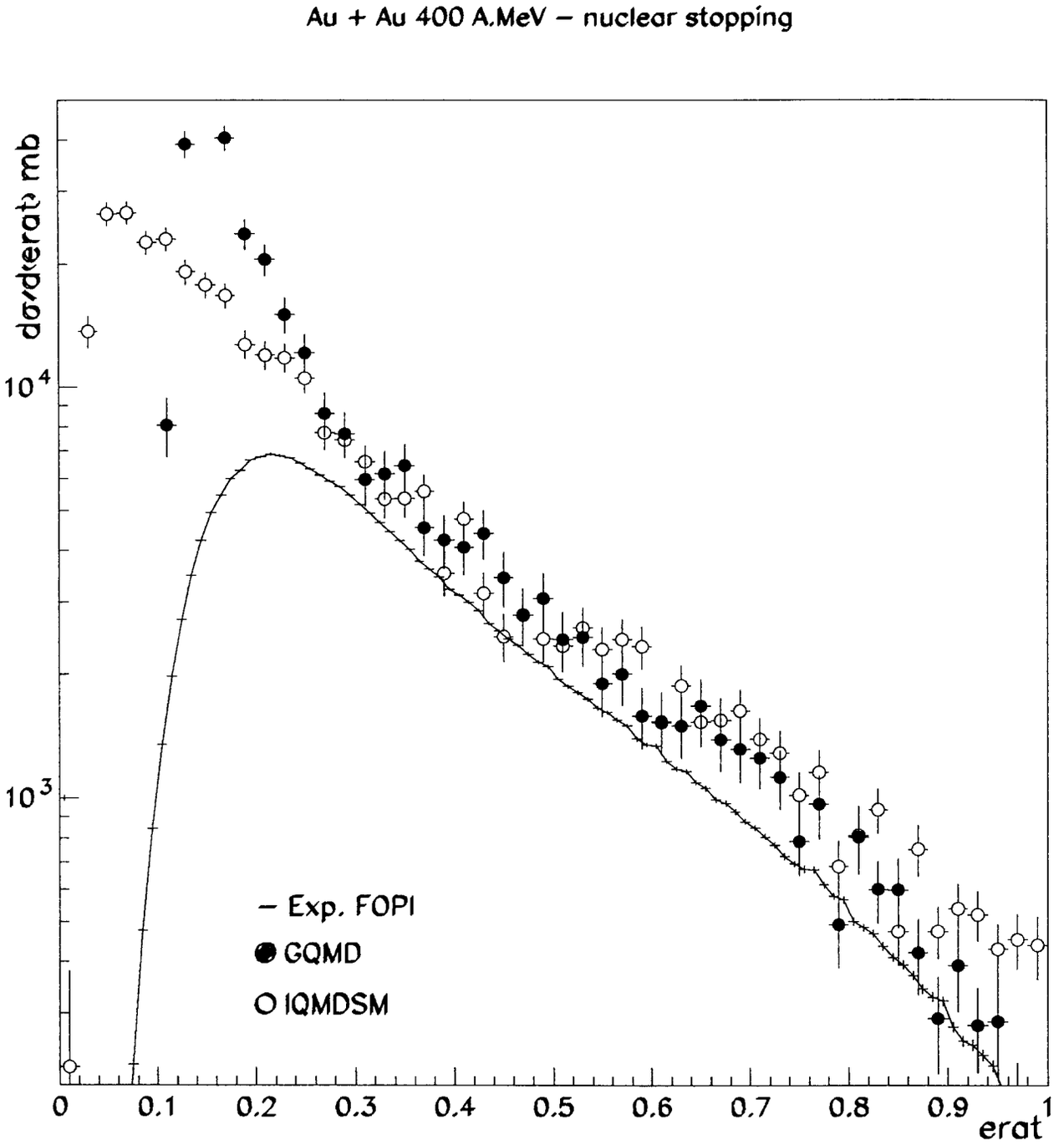
Au + Au 400 A.MeV – nuclear stopping
dσ/derat) mb
10^4
10^3
– Exp. FOPI
GQMD
IQMDSM
0
0.1
0.2
0.3
0.4
0.5
0.6
0.7
0.8
0.9
1
erat

figure I

Au + Au 400 A.MeV – nuclear stopping

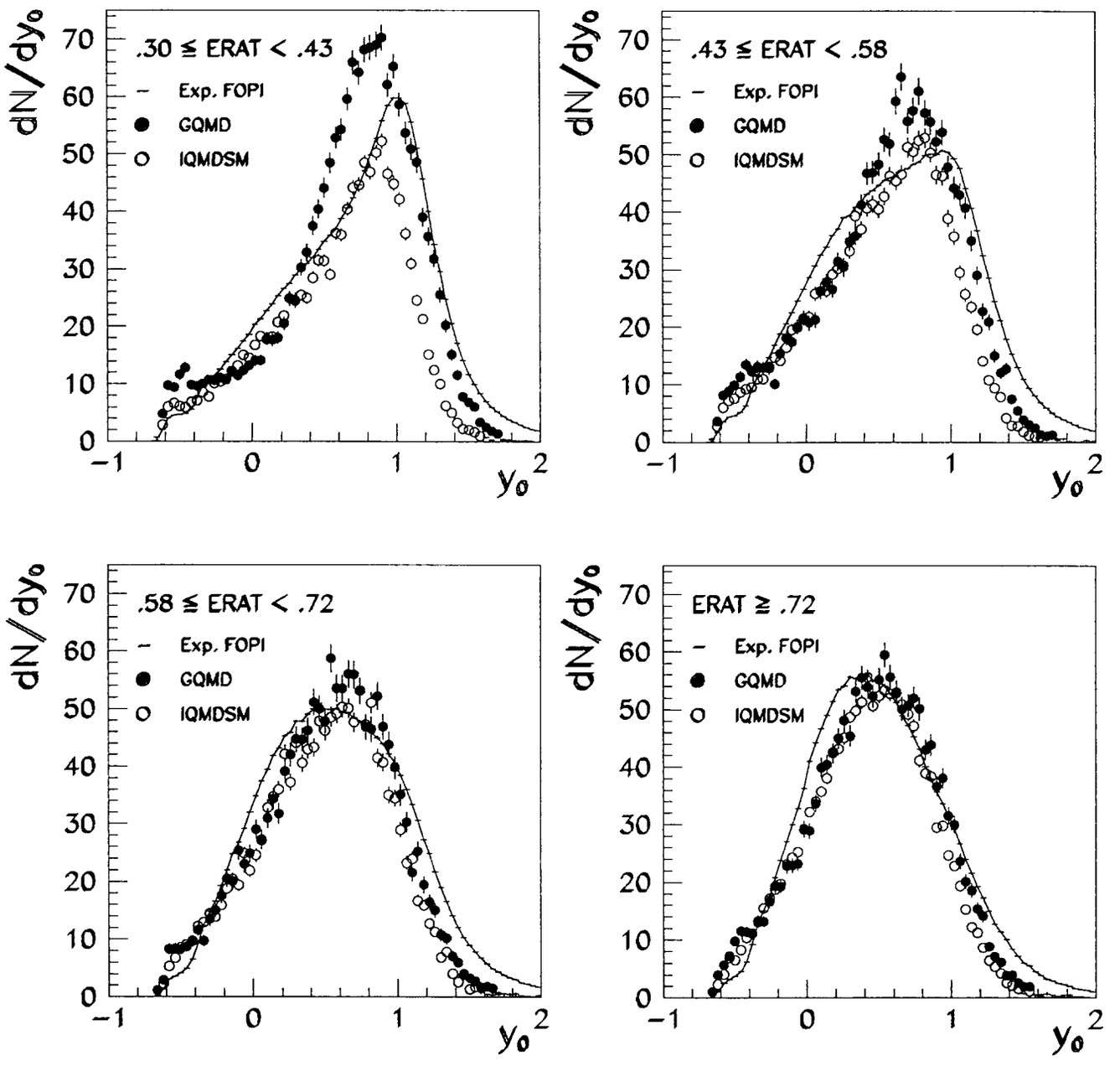

figure II

Au + Au 400 A.MeV – nuclear flow

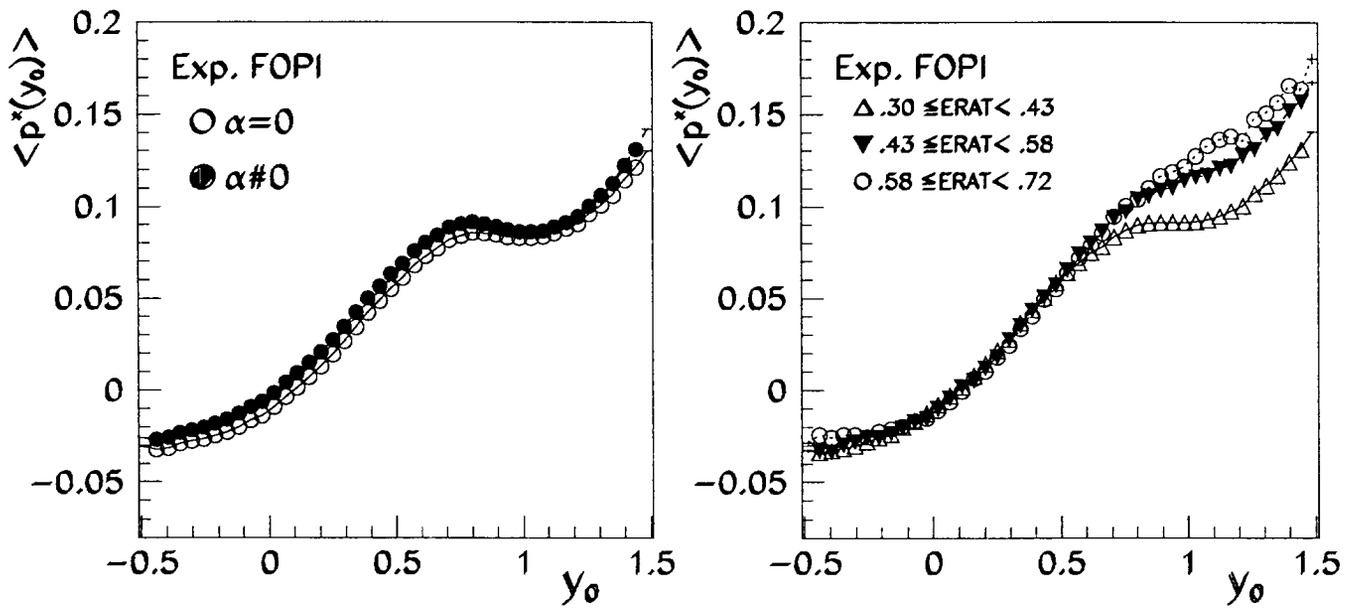

figure III

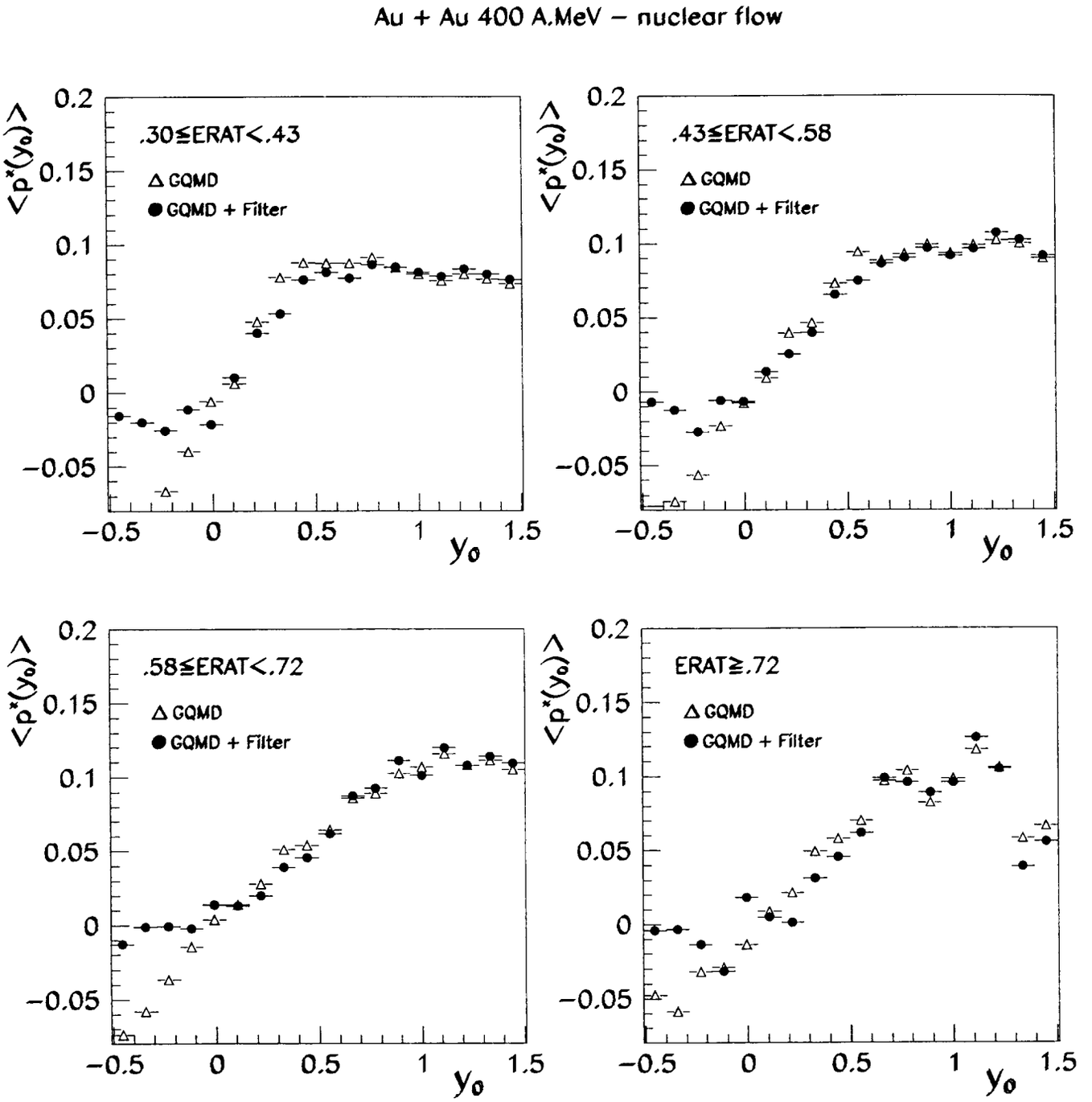
Au + Au 400 A.MeV – nuclear flow
.30≦ERAT<.43
.43≦ERAT<.58
.58≦ERAT<.72
ERAT≧.72
Δ GQMD
● GQMD + Filter
<p*(y0)>
y0

figure IV

Au + Au 400 A.MeV – nuclear flow

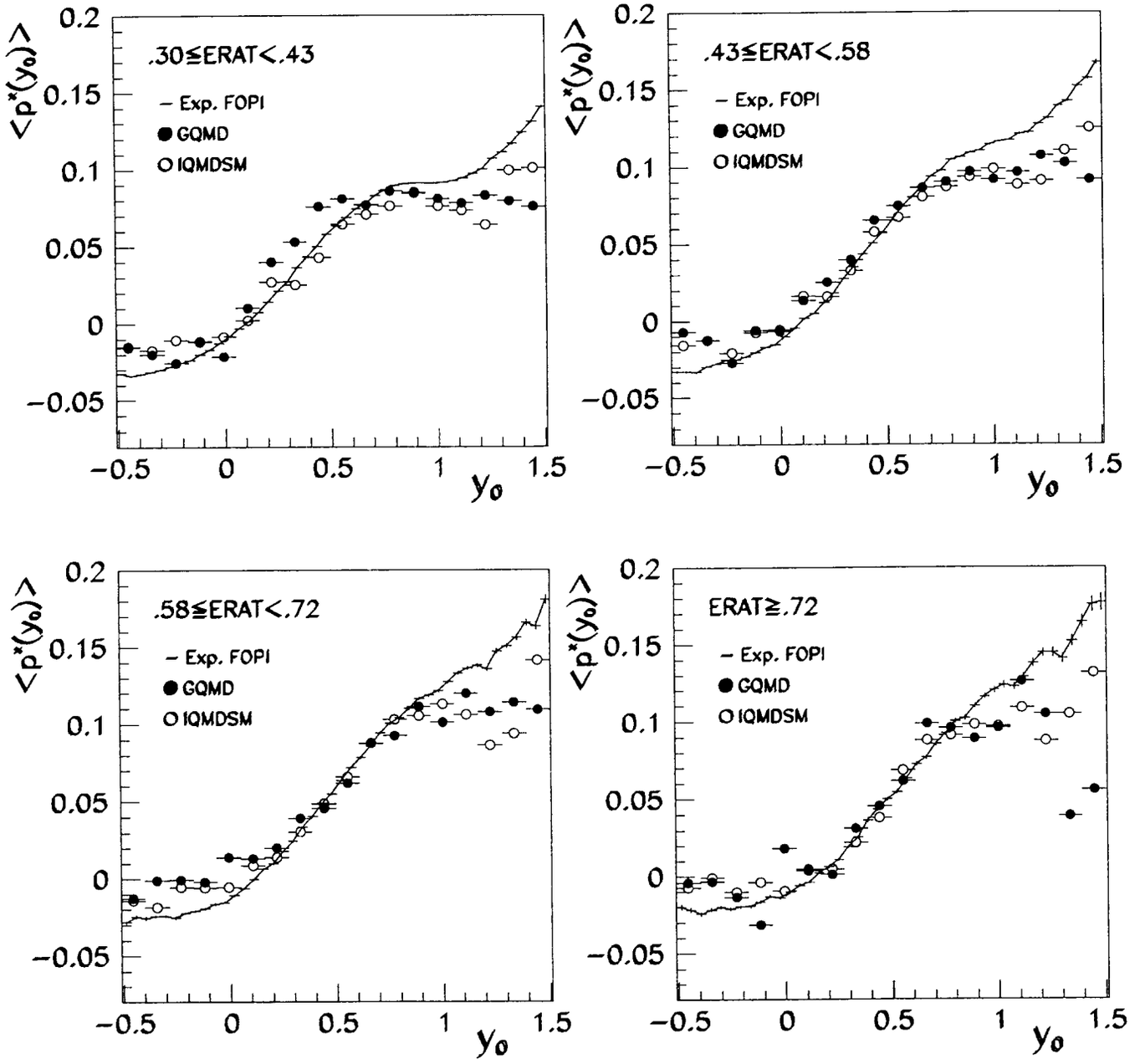

figure V

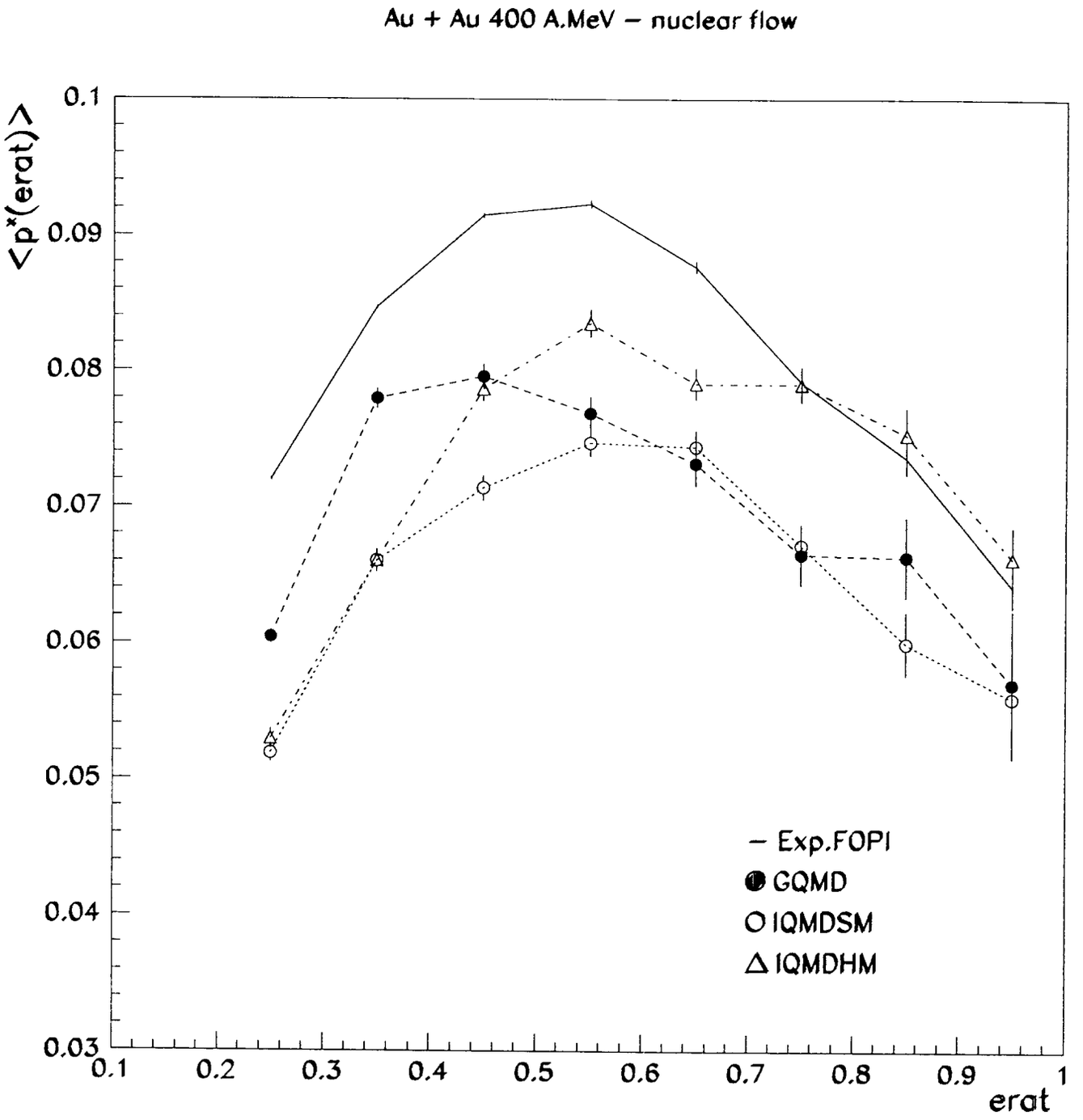
Au + Au 400 A.MeV – nuclear flow
<p*(erat)>
0.1
0.09
0.08
0.07
0.06
0.05
0.04
0.03
0.1
0.2
0.3
0.4
0.5
0.6
0.7
0.8
0.9
1
erat
– Exp.FOPI
GQMD
IQMDSM
IQMDHM

figure VI